THESIS FOR THE DEGREE OF DOCTOR OF PHILOSOPHY IN SOLID AND STRUCTURAL MECHANICS

Multiscale modeling of ductile fracture in solids

ERIK SVENNING

Department of Applied Mechanics
CHALMERS UNIVERSITY OF TECHNOLOGY
Gothenburg, Sweden 2017

Multiscale modeling of ductile fracture in solids
ERIK SVENNING
ISBN 978-91-7597-546-7

Doktorsavhandlingar vid Chalmers tekniska högskola
Ny serie nr. 4227
ISSN 0346-718X
Department of Applied Mechanics
Chalmers University of Technology
SE-412 96 Gothenburg
Sweden
Telephone: +46 (0)31-772 1000

Cover:
Direct numerical simulation of crack propagation: effective stress distribution (left) and magnification of the fractured region, colored by the displacement field (right).

Chalmers Reproservice
Gothenburg, Sweden 2017

Multiscale modeling of ductile fracture in solids
Thesis for the degree of Doctor of Philosophy in Solid and Structural Mechanics
ERIK SVENNING
Department of Applied Mechanics
Chalmers University of Technology

Abstract

Ductile fracture occurs in many situations of engineering relevance, for example metal cutting and crashworthiness applications, where the fracture process is important to understand and predict. Increased understanding can be gained by using multiscale modeling, where the effective response of the material is computed from microscale simulations on Statistical Volume Elements (SVEs)[1] containing explicit models for the nucleation and propagation of microscopic cracks. However, development of accurate and numerically stable models for failure is challenging already on a single scale. In a multiscale setting, the modeling of propagating cracks leads to additional difficulties. Choosing suitable boundary conditions on the SVE is particularly challenging, because conventional boundary conditions (Dirichlet, Neumann and strong periodic) are inaccurate when cracks are present in the SVE. Furthermore, the scale transition relations, i.e. the coupling between the macroscale and the microscale, need to account for the effect of strain localization due to the formation of macroscopic cracks. Even though several approaches to overcome these difficulties have been proposed in the literature, previously proposed models frequently involve explicit assumptions on the constitutive models adopted on the microscale, and require explicit tracking of an effective discontinuity inside the SVE. For the general situation, such explicit discontinuity tracking is cumbersome. Therefore, a multiscale scheme that employs less restrictive assumptions on the microscale constitutive model would be very valuable. To this end, a two-scale model for fracturing solids is developed, whereby macroscale discontinuities are modeled by the eXtended Finite Element Method (XFEM). The model has two key ingredients: *i)* boundary conditions on the SVE that are accurate also when crack propagation occurs in the microstructure, and *ii)* suitable scale transition relations when cracks are present on both scales. Starting from a previously proposed mixed formulation for weakly periodic boundary conditions, effective boundary conditions are developed to obtain accurate results also in the presence of cracks. The modified boundary conditions are combined with smeared macro-to-micro discontinuity transitions, leading to a multiscale modeling scheme capable of handling cracks on both scales. Several numerical examples are given, demonstrating that the proposed scheme is accurate in terms of convergence with increasing SVE size. Furthermore, the good performance of the proposed scheme is demonstrated by comparisons with Direct Numerical Simulations (DNS).

Keywords: XFEM, Computational Homogenization, Weak periodicity, Crack propagation, Fracture, Inf-sup

[1] Sometimes also called Representative Volume Element (RVE) or Microstructural Volume Element (MVE).

Till Annie, Ida och Daniel.

Preface

The work presented in this thesis has been carried out from May 2013 to May 2017 at the Division of Material and Computational Mechanics at Chalmers University of Technology. The research was financially supported by the Swedish Research Council (Vetenskapsrådet) under contract 2012-3006. Some of the simulations presented in this work were performed on resources at Chalmers Centre for Computational Science and Engineering (C3SE) provided by the Swedish National Infrastructure for Computing (SNIC). The models developed in the present work have been implemented in the open source software package OOFEM (www.oofem.org). The help provided and the efforts made by fellow OOFEM developers, in particular Dr. Mikael Öhman, Dr. Carl Sandström, and Dr. Jim Brouzoulis, is greatly appreciated.

I would like to thank my excellent supervisors Associate Professor Martin Fagerström and Professor Fredrik Larsson for sharing their expertise, for their guidance, and for encouragement during these years. I would also like to thank my colleagues for the nice working environment and for many interesting discussions. Finally, I would like to thank my family for their love and support.

Gothenburg, May 2017
Erik Svenning

Thesis

This thesis consists of an extended summary and the following appended papers:

Paper A E. Svenning, M. Fagerström and F. Larsson. Computational homogenization of microfractured continua using weakly periodic boundary conditions. *Computer Methods in Applied Mechanics and Engineering* **299** (2016), 1-21. DOI: 10.1016/j.cma.2015.10.014

Paper B E. Svenning, M. Fagerström and F. Larsson. On computational homogenization of microscale crack propagation. *International Journal for Numerical Methods in Engineering* **108** (2016), 76-90. DOI: 10.1002/nme.5220

Paper C E. Svenning. A weak penalty formulation remedying traction oscillations in interface elements. *Computer Methods in Applied Mechanics and Engineering* **310** (2016), 460-474. DOI: 10.1016/j.cma.2016.07.031

Paper D E. Svenning, M. Fagerström and F. Larsson. Localization aligned weakly periodic boundary conditions. *International Journal for Numerical Methods in Engineering,* in press. DOI: 10.1002/nme.5483

Paper E E. Svenning, F. Larsson and M. Fagerström. Two-scale modeling of fracturing solids using a smeared macro-to-micro discontinuity transition. *Accepted with minor revision for publication in Computational Mechanics.*

Paper F E. Svenning, F. Larsson and M. Fagerström. A two-scale model for strain localization in solids: XFEM procedures and computational aspects. *To be submitted.*

Papers A, B, D, E and F were prepared in collaboration with the co-authors. The author of this thesis was responsible for the major progress of the work, i.e. took part in planning the papers, took part in developing the theory, developed the numerical implementation, carried out the numerical simulations and wrote the papers.

Contents

Part I
Extended Summary

1 Introduction

Ductile fracture occurs in many engineering applications, for example in metal cutting or when structures are subjected to crash loading. In such applications, good control of the fracture process is often needed to ensure safe and efficient operation. Hence, a good prediction of the entire fracture process, including the post peak-load behavior, is important and a good understanding of the underlying mechanisms is needed. Since fracture starts with nucleation of voids and microcracks that grow and coalesce to eventually form macroscopic cracks, increased understanding may be gained by studying the microstructure of the material using suitable modeling techniques. In principle, this could be done by explicitly resolving the microstructure of the material everywhere in the specimen, i.e. Direct Numerical Simulation (DNS). Unfortunately, this approach often leads to unacceptable computational cost. Therefore, the effective behavior of the microstructure is often predicted by means of computational homogenization, see e.g. Zohdi and Wriggers [1], Fish et al. [2], Ostoja-Starzewski [3], Kouznetsova et al. [4], Talebi et al. [5], the reviews by Geers et al. [6] and Nguyen et al. [7], or the text book by Zohdi and Wriggers [8]. In computational homogenization, a key step is the computation of the homogenized microscale response in a Statistical Volume Element (SVE)[1] with suitable Boundary Conditions (BCs). However, modeling of fracture in a computational homogenization setting turns out to be very challenging and several issues need to be addressed, including *i)* pathological SVE size and mesh size dependence of first order homogenization in the presence of macroscale strain localization, *ii)* the choice of suitable BCs on the SVE and *iii)* the choice of robust and accurate fracture models on the microscale.

Regarding the pathological SVE size and mesh size dependence, it is well known that this follows from standard first order homogenization when strain localization occurs inside the SVE. More precisely, first order homogenization in the presence of microscale damage evolution corresponds to a local continuum damage model on the macroscale and therefore suffers from the well documented pathological mesh size sensitivity characteristic for such damage models, see e.g. [10, 11]. To circumvent these problems, a suitable model that incorporates a length scale is needed for the macroscopic representation of the localization zone. A popular choice is to inject a macroscopic discontinuity into the model when some localization criterion is fulfilled [7], whereby the failure can be represented by means of cohesive zone elements [12, 13], the eXtended Finite Element Method (XFEM) [14, 5, 15, 16] or embedded discontinuities [17, 18, 19]. Alternatively, the localized crack may be resolved explicitly on the macroscale using a suitable adaptive scheme along the lines in

[1] In the literature, both *Representative Volume Element (RVE)* and *Microstructural Volume Element (MVE)*, cf. [9], are also used to denote a sample of the microstructure. To stress the fact that a sample of finite size will, in general, not be truly representative, we prefer the notion *Statistical Volume Element (SVE)*, cf. Ostoja-Starzewski [3].

[20], or second order homogenization [4] may be employed. Even though much research effort has been devoted to the development of multiscale localization schemes, there are still challenges remaining. Previously proposed schemes generally involve restrictive assumptions on the models adopted on the microscale and require explicit tracking of a damaged zone inside the SVE. However, such explicit tracking may be cumbersome or impossible when complex fracture models are employed on the microscale. Therefore, a scheme that does not require explicit tracking of the localized zone inside the SVE would be very valuable.

Regarding the choice of suitable boundary conditions on the SVE, this turns out to be critical when crack nucleation and propagation occurs inside the SVE. This observation holds also prior to localization, i.e. at the early stage of damage progression. More precisely, it is well known that conventional BCs (Neumann, Dirichlet and strong periodic) are inaccurate if cracks intersect the SVE boundary, see the illustration in Paper A and the discussion in [5, 9]. Even though efforts have been made to develop BCs that perform better than conventional BCs [9, 17], there is potential for improved performance by developing BCs that are adapted to the geometry at hand.

For the choice of microscale fracture model, it should be noted that modeling of ductile fracture is challenging also on a single scale, and a wide range of modeling approaches have been developed, see e.g. Miehe et al. [21], Ortiz and Pandolfi [22], Belytschko and Black [23], the XFEM review by Fries and Belytschko [24], the lecture notes by Jirasek [10], or the text book by Lemaitre [25]. For the representation of the damaged zone, one option is to model it in a smeared sense, using local[2] or nonlocal continuum damage models, or phase field models. Using such models allows for modeling of complex damage patterns without additional geometrical difficulties, but a very fine mesh is needed to accurately represent a discrete crack. An alternative frequently used in commercial codes is element removal techniques, where finite elements are removed from the numerical simulation when a predefined damage threshold is exceeded. Such models are appealingly simple, but require scaling of the damage evolution model to avoid pathological mesh dependence. To overcome these difficulties, a discrete crack model may be used instead, such as element embedded discontinuities, interface elements or XFEM. These discrete models introduce additional geometrical difficulties (explicit representation and tracking of the crack front), but allow for modeling of sharp cracks. Regardless of the approach chosen for representation of the damaged zone, the progression of damage needs to be modeled in a suitable way. For example, damage progression may be modeled as a function of the stress or the plastic strain in the material. In particular, several authors have explored the possibilities of combining element embedded discontinuities or XFEM with fracture criteria based on stress intensity factors [26, 27], material crack driving force [28], stress [29, 30], plastic strain [31] or loss of ellipticity [32].

To summarize, successful multiscale modeling of ductile fracture requires accurate BCs on the SVE and consistent scale transition relations as well as robust and accurate models for propagating cracks. In the present work, we adopt the concept of Variationally Consistent Homogenization (VCH) [20, 33] to derive scale transition relations and develop weakly periodic boundary conditions that can be applied on SVEs containing cracks. For the representation of propagating cracks, we mainly use XFEM.

[2]With suitable regularization, typically element size scaling.

2 Aim of research

The aim of the present work is to develop a multiscale model suitable for ductile fracture. As indicated above, such models need to include the following components:

1. A suitable scale bridging scheme capable of handling macroscale localization.
2. Suitable boundary conditions on the Statistical Volume Element (SVE) in the presence of cracks in the SVE.
3. Suitable fracture models on the microscale.

In the present work, models proposed in the literature are adopted for *3)*, whereas novel techniques are developed for *1)* and *2)*.

3 A fracturing continuum

3.1 Model problem

Before developing the multiscale modeling scheme, we first establish the weak form of the resolved problem (i.e. prior to the introduction of computational homogenization) for a continuum containing propagating cracks. To this end, consider a domain Ω with external boundary Γ_{ext} and internal boundaries Γ_{int}, where Γ_{int} may for example represent cracks as indicated in Figure 3.1a or grain boundaries as indicated in Figure 3.1b. The internal boundaries Γ_{int} have a predefined normal $\boldsymbol{n}_{int}$ and consist of two-sided surfaces, with a positive side Γ_{int}^{+} and a negative side Γ_{int}^{-} as also indicated in Figure 3.1. The external boundary consists of a part $\Gamma_{ext,D}$ with Dirichlet boundary conditions and a part $\Gamma_{ext,N}$ with Neumann boundary conditions. The boundary of Ω is therefore decomposed as $\partial\Omega = \Gamma_{ext,D} \cup \Gamma_{ext,N} \cup \Gamma_{int}$. Letting superscripts $^{+}$ and $^{-}$ denote quantities on Γ_{int}^{+} and Γ_{int}^{-}, respectively, we define the normal $\boldsymbol{n}_{int}$ to be the outward unit normal on Γ_{int}^{-}, i.e. $\boldsymbol{n}_{int} \stackrel{\text{def}}{=} \boldsymbol{n}_{int}^{-}$. As indicated in Figure 3.1, the internal boundaries may branch and intersect and, hence, $\boldsymbol{n}_{int}$ is not necessarily continuous along an arbitrary part of Γ_{int}, not even prior to introducing a finite element discretization.

Considering small strains and quasistatic loading, the strong form of the equilibrium equations is given by

$$\begin{aligned} -\boldsymbol{\sigma}\cdot\boldsymbol{\nabla} &= \boldsymbol{0} \text{ in } \Omega, \\ \boldsymbol{t}^{+} + \boldsymbol{t}^{-} &= \boldsymbol{0} \text{ on } \Gamma_{int}, \\ \boldsymbol{t} \stackrel{\text{def}}{=} \boldsymbol{\sigma}\cdot\boldsymbol{n} &= \hat{\boldsymbol{t}} \text{ on } \Gamma_{ext,N}, \\ \boldsymbol{u} &= \hat{\boldsymbol{u}} \text{ on } \Gamma_{ext,D}, \end{aligned} \tag{3.1}$$

where $\boldsymbol{\sigma}$ is the Cauchy stress, $\boldsymbol{\nabla}$ is the gradient operator, $\boldsymbol{n}$ is a unit normal vector, $\hat{\boldsymbol{t}}$ is a prescribed traction and $\hat{\boldsymbol{u}}$ is a prescribed displacement. Furthermore, letting $\boldsymbol{\epsilon} \stackrel{\text{def}}{=} (\boldsymbol{u}\otimes\boldsymbol{\nabla})^{sym}$ and $[\![\boldsymbol{u}]\!] \stackrel{\text{def}}{=} \boldsymbol{u}^{+} - \boldsymbol{u}^{-}$, constitutive models are given for the stress-strain

relation $\boldsymbol{\sigma} = \boldsymbol{\sigma}\{\boldsymbol{\epsilon}\}$ and the traction-separation law $\boldsymbol{t} = \boldsymbol{t}\{[\![\boldsymbol{u}]\!]\}$, where the dependence of $\boldsymbol{\sigma}$ and $\boldsymbol{t}$ on internal variables has been omitted for brevity.

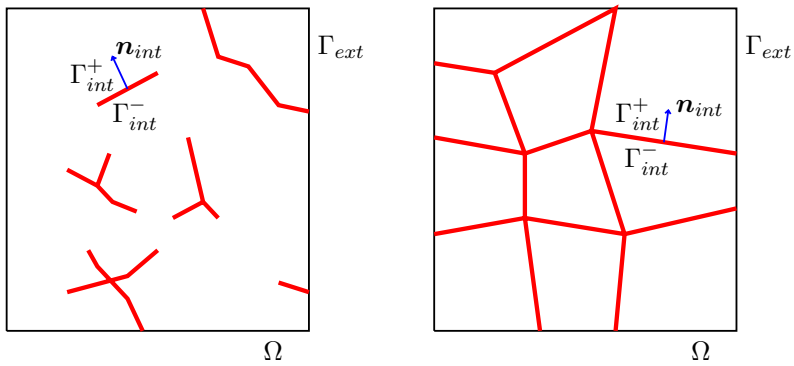

(a) *Cracks.* (b) *Grain boundaries.*

Figure 3.1: *Specimen with internal boundaries.*

The (one field) weak solution corresponding to Equation (3.1) is obtained by finding $\boldsymbol{u} \in \mathbb{U}$ such that

$$\int_\Omega \boldsymbol{\sigma}\{\boldsymbol{\epsilon}\} : [\delta\boldsymbol{u} \otimes \boldsymbol{\nabla}] \, \mathrm{d}\Omega - \int_{\Gamma_{int}} \boldsymbol{t}\{[\![\boldsymbol{u}]\!]\} \cdot [\![\delta\boldsymbol{u}]\!] \, \mathrm{d}\Gamma = \int_{\Gamma_{ext,N}} \hat{\boldsymbol{t}} \cdot \delta\boldsymbol{u} \, \mathrm{d}\Gamma \; \forall \delta\boldsymbol{u} \in \mathbb{U}^0$$

$$\mathbb{U} = \left\{ \boldsymbol{v} : \boldsymbol{v} \in \left[\mathbb{H}^1(\Omega)\right]^d, \; \boldsymbol{v} = \hat{\boldsymbol{u}} \text{ on } \Gamma_{ext,D} \right\},$$

$$\mathbb{U}^0 = \left\{ \boldsymbol{v} : \boldsymbol{v} \in \left[\mathbb{H}^1(\Omega)\right]^d, \; \boldsymbol{v} = \boldsymbol{0} \text{ on } \Gamma_{ext,D} \right\}, \tag{3.2}$$

where $\mathbb{H}^1(\Omega)$ is the space of square integrable functions with square integrable derivatives in Ω, and d is the number of spatial dimensions. We note that the cohesive zone law $\boldsymbol{t}\{[\![\boldsymbol{u}]\!]\}$ is given on stiffness format, thereby allowing softening to be included in the cohesive zone law in a straightforward manner.

3.2 Representation of internal boundaries

General remarks

The internal boundaries Γ_{int} in Equation (3.2) can be represented in different ways, either by means of interface elements in a mesh that is adapted to the internal boundaries, by means of embedded discontinuities, or by using XFEM. In principle, any of these three interface models could have been used in the present study. In the following, a few comments are given on XFEM and interface elements, two methods that have both been used in the present work.

Interface elements

A simple way to represent interfaces in a material is to use interface elements, see for example the pioneering work in [34], or [35] for a textbook. This approach has the advantage of easy implementation, and can be readily applied if the crack propagation direction can be determined a-priori, for example when considering debonding between material phases. If the crack path is not known in advance, interface elements may be inserted between all bulk elements [36], or remeshing may be applied [37]. Even though interface elements can be used to treat arbitrary crack propagation, there are serious drawbacks due to increased computational cost and potentially cumbersome remeshing. Furthermore, interface elements between all bulk elements introduce artificial compliance in the structure. An additional concern is that interface elements may lead to overestimation of the energy dissipation due to incorrect crack length. Nevertheless, the use of interface elements to model fracture is an active field of research, and recent developments include, for example, self adaptive elements [38] in order to allow a coarser discretization.

The eXtended Finite Element Method (XFEM)

A drawback of crack modeling by means of interface elements is that the cracks are restricted by the bulk mesh. To circumvent this restriction, and allow arbitrary crack propagation independent of the underlying mesh, XFEM can be used [23, 24]. The key feature of XFEM is that the approximation space for the primary variable is enriched locally in some parts of the domain. For crack propagation problems, the displacement approximation is enriched according to

$$\boldsymbol{u}^h = \sum_{i \in I} N_i(\boldsymbol{x}) \boldsymbol{a}_i + \sum_{j \in J} \sum_{i \in I_j^*} N_i^*(\boldsymbol{x}) \left[\Psi^j(\boldsymbol{x}) - \Psi^j(\boldsymbol{x}_i) \right] \boldsymbol{b}_i^j, \tag{3.3}$$

where N_i are the standard basis functions, $\boldsymbol{a}_i$ are the standard nodal degrees of freedom (dofs), N_i^* are the enriched basis functions, $\boldsymbol{b}_i^j$ are the enriched nodal dofs, and the functions Ψ^j describe the enrichments. Furthermore, I is the set of all nodes, J denotes a set of enrichments, and I_j^* is the set of enriched nodes for enrichment j. We note that the XFEM contribution contains the term $\left[\Psi^j(\boldsymbol{x}) - \Psi^j(\boldsymbol{x}_i)\right]$ rather than only $\Psi^j(\boldsymbol{x})$, i.e. the enrichment is shifted by the nodal level set value. In this way, the Kronecker-delta property of the discretization is preserved [39].

Regarding the explicit expressions for the enrichment functions Ψ^j, it is convenient to formulate these functions in terms of level set fields. To this end, we define $\Phi(\boldsymbol{x})$ as the normal signed distance to the crack and $\gamma(\boldsymbol{x})$ as the tangential signed distance to the crack. For elements completely cut by a crack, a suitable choice is to use sign (or, equivalently, Heaviside) enrichment, whereby Ψ is given by

$$\Psi = \operatorname{sgn}\left(\Phi(\boldsymbol{x})\right). \tag{3.4}$$

Even though sign enrichment can be used also in elements containing crack tips, it leads to poor accuracy in the predicted stress field if the mesh is not extremely fine, especially for elastic problems. Improved accuracy can be obtained by enriching with asymptotic

functions in elements containing crack tips as illustrated in Figure 3.2, cf. [40]. For elasticity problems, the analytic solution for linear elastic fracture mechanics can be used, whereby the crack tip enrichments take the form

$$\begin{aligned}\Psi_1 &= \sqrt{r}\sin(\theta/2),\\ \Psi_2 &= \sqrt{r}\sin(\theta/2)\sin(\theta),\\ \Psi_3 &= \sqrt{r}\cos(\theta/2),\\ \Psi_4 &= \sqrt{r}\cos(\theta/2)\sin(\theta).\end{aligned} \tag{3.5}$$

For cohesive cracks (i.e. cracks that are not traction free), asymptotic functions that differ slightly from Equation (3.5) can be used, see e.g. [26]. Furthermore, if branching or intersecting cracks are considered, it is not sufficient to add enrichments for each crack separately. The crack intersections need special treatment, e.g. by using so called *junction functions* [41].

So far, the practical computation of the level set functions Φ and γ has not been specified. Here, three options are possible. We may

1. compute the level set functions directly from an explicit crack representation (e.g. a polygon in 2D or a triangulation in 3D),

2. use an explicit crack representation to evaluate the level set functions in the nodes, and then use the standard basis functions to interpolate Φ and γ, or

3. use only level set functions stored in nodes.

In this thesis, alternative 2 has been considered, i.e. a hybrid representation, where a polygon representation is used to compute the necessary level set fields [42]. This choice is convenient and computationally efficient.

To summarize, the present work employs a crack model based on XFEM with a hybrid geometry representation as stated above. Crack intersections are handled using *junction functions* [41]. A shifted enrichment is employed to preserve the Kronecker-delta property and elements containing a crack tip are enriched with asymptotic functions.

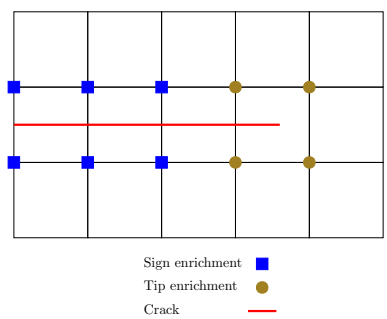

Figure 3.2: *XFEM enrichment around a crack: sign enrichment is used in elements completely cut by the crack, whereas special tip enrichments are used in elements containing crack tips.*

Stability of interface models

When modeling fracture by means of discrete crack models such as interface elements or XFEM, it is common to model the damage process by means of an initially elastic cohesive zone with progressing damage. However, for such cohesive zone models with high initial stiffness, it is well known that traction oscillations may occur along the interface [43, 44, 45]. A frequently used strategy to alleviate this problem is to employ reduced Lobatto integration of the cohesive traction along the interface. Even though this strategy has been shown to work well for straight cracks [43], it is shown in Paper C that severe traction oscillations may occur for curved and/or intersecting cracks. Interestingly, it turns out that these traction oscillations can be explained by analyzing the stability properties of a corresponding mixed formulation. In particular, reduced Lobatto integration corresponds to a traction approximation that violates the inf-sup (LBB) condition, and this explains the occurrence of traction oscillations. Furthermore, both full (Gauss) integration and one-point integration correspond to traction approximations violating the inf-sup condition, thereby leading to traction oscillations. As shown in Paper C, it is possible overcome this issue by instead using a weak penalty formulation, where the cohesive zone contribution is projected onto a stable reduced approximation space. This reduced space can, for example, be a piecewise constant traction approximation in combination with a piecewise quadratic displacement approximation. See Paper C for further details.

Crack initiation and propagation

Crack initiation and propagation can be modeled by combining a suitable representation of the crack geometry (XFEM, interface elements, remeshing) with criteria for the onset and direction of crack growth. Without attempting to list all developments in the field, we first note that models describing crack propagation are not fundamentally tied to the chosen crack representation. For example, crack propagation based on stress intensity factors was studied by Zi and Belytschko [27] using XFEM, whereas Khoei et al. [46] employed a remeshing technique. Other examples of crack propagation based on stress intensity factors or material forces can be found in [47, 48, 49] as well as the comparison between different approaches in [26]. Furthermore, crack propagation in combination with plasticity and damage in the bulk material has been studied by many authors, using propagation models based on the stress [29, 50] or the plastic strain [31] around the crack tip. When damage in the bulk material is considered, crack initiation models may also be based on the loss of ellipticity of the material tangent stiffness, see e.g. [15, 35, 51]. In the latter case, crack initiation is predicted when the tangent stiffness is singular (strict ellipticity condition) or when the so-called acoustic tensor is singular. These two criteria both allow the direction of the discontinuity to be identified.

In the numerical examples presented in this thesis, propagation of XFEM cracks on the microscale is mainly modeled using the concept of material forces. Branch enrichment is used in elements containing crack tips in order to make the material force evaluation sufficiently insensitive to the mesh size and to the radius used in the domain integral evaluation. We note, however, that the framework developed here is not restricted to a particular choice of crack propagation model. The crack propagation model based on material forces can easily be replaced by a criterion based on e.g. plastic deformation

around the crack tip. For macroscale discontinuity insertion (Paper F), we consider loss of ellipticity of the material tangent stiffness, see Section 4.4 for further comments.

4 Macroscale problem

4.1 Preliminaries

As stated previously, the main objective of the present work is to develop a scheme for multiscale localization, including suitable BCs on the SVE and a consistent scale bridging scheme. To this end, we employ the concept of VCH [52, 33] and use weakly periodic BCs [53] that are tailored to the problem at hand by adapting the traction discretization to the topology of the SVE problem (Paper A and Paper B). For the later stage of damage progression, it turns out that weakly periodic BCs can be conveniently aligned to an identified localization direction (Paper D).

When localization occurs inside the SVE, it is necessary to account for the corresponding macroscale discontinuity by developing a suitable scale bridging scheme (Paper E and Paper F). In the present work, we employ a strong discontinuity on the macroscale and consider the macroscale displacement jump as smeared over the SVE, thereby avoiding the need to explicitly split the SVE response into a continuous part and a discontinuous part. In the following, VCH for standard first order homogenization is described. Next, the proposed multiscale localization scheme is outlined and a few comments on the method are given.

4.2 Variationally Consistent Homogenization (VCH)

To develop VCH for standard first order homogenization, consider a macroscopically homogeneous solid with domain $\bar{\Omega}$ as shown in Figure 4.1. Studying the solid in greater detail reveals the heterogeneous microstructure of the material, here illustrated as microcracks, as also shown in Figure 4.1. Even though the material is heterogeneous on the microscale, we wish to solve for the smooth (macroscale) displacement $\bar{\boldsymbol{u}}$ without explicitly resolving the microstructure on the macroscale. To take advantage of the different scales present in the problem, we may split the displacement $\boldsymbol{u}$ into a macroscale part $\boldsymbol{u}^{\mathrm{M}}$, which explicitly depends on $\bar{\boldsymbol{u}}$, and a microscale part $\boldsymbol{u}^{\mathrm{s}}$, according to $\boldsymbol{u} = \boldsymbol{u}^{\mathrm{M}} + \boldsymbol{u}^{\mathrm{s}}$. Assuming the same split for the test functions, we can state the original problem in Equation (3.2) as the *macro problem*

$$\int_{\Omega} \boldsymbol{\sigma} : \left[\delta \boldsymbol{u}^{\mathrm{M}} \otimes \boldsymbol{\nabla}\right] \mathrm{d}\Omega - \int_{\Gamma^{+}_{int}} \boldsymbol{t} \cdot \left[\!\left[\delta \boldsymbol{u}^{\mathrm{M}}\right]\!\right] \mathrm{d}\Gamma = \int_{\Gamma_{ext,N}} \hat{\boldsymbol{t}} \cdot \delta \boldsymbol{u}^{\mathrm{M}} \, \mathrm{d}\Gamma \; \forall \delta \boldsymbol{u}^{\mathrm{M}} \in \mathbb{U}^{\mathrm{M},0}, \tag{4.1}$$

and the *micro problem*

$$\int_{\Omega} \boldsymbol{\sigma} : \left[\delta \boldsymbol{u}^{\mathrm{s}} \otimes \boldsymbol{\nabla}\right] \mathrm{d}\Omega - \int_{\Gamma^{+}_{int}} \boldsymbol{t} \cdot \left[\!\left[\delta \boldsymbol{u}^{\mathrm{s}}\right]\!\right] \mathrm{d}\Gamma = \int_{\Gamma_{ext,N}} \hat{\boldsymbol{t}} \cdot \delta \boldsymbol{u}^{\mathrm{s}} \, \mathrm{d}\Gamma \; \forall \delta \boldsymbol{u}^{\mathrm{s}} \in \mathbb{U}^{\mathrm{s}}, \tag{4.2}$$

respectively. Here, $\mathbb{U}^{\mathrm{M},0}$ and $\mathbb{U}^{\mathrm{s}}$ represent suitable test spaces. So far, we have introduced a split of the displacement field, but we have not yet introduced computational homogenization based on SVEs: Equations (4.1) and (4.2) pertain to the Variational MultiScale method (VMS) introduced by Hughes et al. [54].

The second step of VCH is to restate the integrals in Equation (4.1) using running averages in order to obtain a homogenized problem. To this end, we consider the macroscopically homogeneous domain $\bar{\Omega} = \Omega \cup \Gamma_{int}$ and introduce the approximation

$$\begin{aligned} \int_{\Omega} f \,\mathrm{d}\Omega + \int_{\Gamma_{int}} g \,\mathrm{d}\Gamma &\approx \int_{\bar{\Omega}} f_{\square} \,\mathrm{d}\Omega, \\ f_{\square} \overset{\text{def}}{=} \frac{1}{|\Omega_{\square}|} &\left[\int_{\Omega_{\square}} f \,\mathrm{d}\Omega + \int_{\Gamma_{int} \cap \Omega_{\square}} g \,\mathrm{d}\Gamma \right], \end{aligned} \tag{4.3}$$

where $\Omega_{\square}$ denotes an SVE.

Finally, prolongation conditions defining $\boldsymbol{u}^{\mathrm{M}}$ in terms of $\bar{\boldsymbol{u}}$ need to be specified. The standard approach is to employ first order homogenization, whereby $\boldsymbol{u}^{\mathrm{M}}$ varies linearly over the SVE according to

$$\boldsymbol{u}^{\mathrm{M}} = \bar{\boldsymbol{\epsilon}} \cdot [\boldsymbol{x} - \bar{\boldsymbol{x}}] \;\text{ inside } \Omega_{\square}(\bar{\boldsymbol{x}}),\; \forall \bar{\boldsymbol{x}} \in \bar{\Omega}, \tag{4.4}$$

where $\bar{\boldsymbol{x}} = \frac{1}{|\Omega_{\square}|} \int_{\Omega_{\square}} \boldsymbol{x} \,\mathrm{d}\Omega$ and $\bar{\boldsymbol{\epsilon}} = (\bar{\boldsymbol{u}} \otimes \boldsymbol{\nabla})^{sym}|_{\boldsymbol{x}=\bar{\boldsymbol{x}}}$ is the symmetric part of the displacement gradient evaluated at $\bar{\boldsymbol{x}}$. See Figure 4.2 for a schematic illustration. For first order

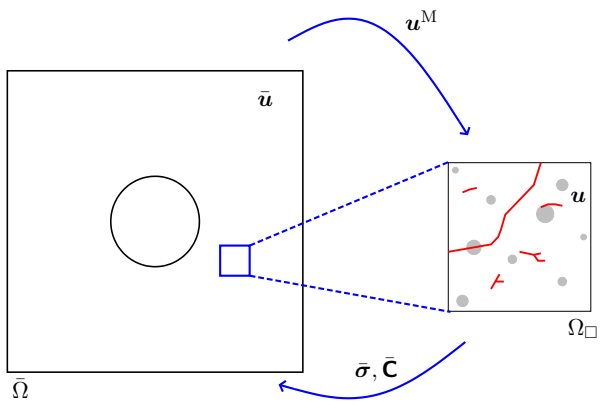

Figure 4.1: *Macroscopically homogeneous solid with heterogeneous microstructure. Using computational homogenization implies solving for the smooth displacement field $\bar{\boldsymbol{u}}$ on the macroscale. The macroscopic part $\boldsymbol{u}^{\mathrm{M}}(\bar{\boldsymbol{u}})$ of the displacement in the SVE is imposed via suitable boundary conditions and the SVE solution provides the effective macroscale stress $\bar{\boldsymbol{\sigma}}$ and the tangent $\bar{\mathbf{C}} = \frac{\partial \bar{\boldsymbol{\sigma}}}{\partial \bar{\boldsymbol{\epsilon}}}$.*

homogenization, we may now restate Equation (4.1) as the macroscale problem of finding

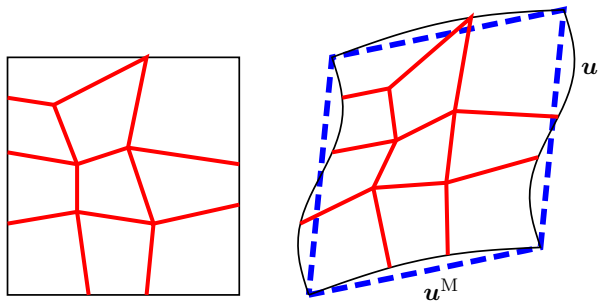

Figure 4.2: *First order homogenization:* $\boldsymbol{u}^{\mathrm{M}}$ *varies linearly within the SVE.*

$\bar{\boldsymbol{u}} \in \bar{\mathbb{U}}$ such that

$$\int_{\bar{\Omega}} \bar{\boldsymbol{\sigma}}\{\bar{\boldsymbol{\epsilon}}\} : \delta\bar{\boldsymbol{\epsilon}} \, \mathrm{d}\Omega = \int_{\Gamma_{ext,N}} \hat{\boldsymbol{t}} \cdot \delta\bar{\boldsymbol{u}} \, \mathrm{d}\Gamma \quad \forall \delta\bar{\boldsymbol{u}} \in \bar{\mathbb{U}}^0, \tag{4.5}$$

where $\bar{\mathbb{U}}$ and $\bar{\mathbb{U}}^0$ are the trial and test spaces for the homogenized problem, and where the effective macroscale stress $\bar{\boldsymbol{\sigma}}$ is obtained from the microscale solution according to

$$\bar{\boldsymbol{\sigma}} \stackrel{\mathrm{def}}{=} \frac{1}{|\Omega_{\square}|} \int_{\Omega_{\square}} \boldsymbol{\sigma} \, \mathrm{d}\Omega. \tag{4.6}$$

More precisely, in each macroscale point, we first evaluate $\bar{\boldsymbol{\epsilon}}$ from the current guess for $\bar{\boldsymbol{u}}$. $\bar{\boldsymbol{\epsilon}}$ is imposed on the SVE using suitable boundary conditions, and the macroscale stress $\bar{\boldsymbol{\sigma}}$ is computed from Equation (4.6), cf. Figure 4.1. For brevity, we again use the algorithmic notation $\bar{\boldsymbol{\sigma}}\{\bar{\boldsymbol{\epsilon}}\}$ omitting the possible dependence on internal variables.

4.3 Smeared macro-to-micro transitions

When strain localization occurs, first order homogenization as given by Equation (4.5) is inappropriate. More precisely, first order homogenization corresponds to a local continuum damage model with pathological dependence on the macroscale mesh size and the SVE size. To overcome this problem, we consider the split of the domain $\bar{\Omega} = \bar{\Omega}_r \cup \bar{\Omega}_d$ as indicated in Figure 4.3. Here, $\bar{\Omega}_r$ denotes the regular domain where macroscopic localization does not occur, and $\bar{\Omega}_d$ denotes the discontinuity region where macroscopic localization needs to be accounted for. In particular, we will assume that $\bar{\Omega}_d$ can be described by a mean interface $\bar{\Gamma}_d$ and a thickness l_d. For the regular domain $\bar{\Omega}_r$, we still use the approximation given by Equation (4.3). However, for the discontinuity region $\bar{\Omega}_d$, we state the integrals based on the interface $\bar{\Gamma}_d$ according to

$$\int_{\bar{\Omega}_d} f \, \mathrm{d}\Omega + \int_{\Gamma^+_{int} \cap \bar{\Omega}_d} g \, \mathrm{d}\Gamma \approx \int_{\bar{\Omega}_d} f_{\square} \, \mathrm{d}\Omega \approx \int_{\bar{\Gamma}_d} l_d f_{\square} \, \mathrm{d}\Gamma, \tag{4.7}$$

where the last approximation is based on the assumption of a narrow region $\bar{\Omega}_d$, i.e. we assume that l_d is sufficiently small so that the integral over $\bar{\Omega}_d$ may be replaced by an integral over $\bar{\Gamma}_d$.

In the presence of localization, $f_\square$ in Equation (4.7) will not be representative if evaluated on an arbitrarily sized SVE $\Omega_\square$. In $\bar{\Omega}_d$, we therefore consider homogenization only along $\bar{\Gamma}_d$, whereas the direction perpendicular to $\bar{\Gamma}_d$ is fully resolved. In practice, this is achieved by choosing l_d such that it matches the SVE size (see Paper E for explicit expressions).

For the prolongation conditions, different expressions will be employed for $\bar{\Omega}_r$ and $\bar{\Omega}_d$. We assume that the homogenized displacement ansatz $\bar{\boldsymbol{u}} \in \bar{\mathbb{U}}$ is smooth on $\hat{\Omega} \stackrel{\text{def}}{=} \bar{\Omega}_r \cup \bar{\Omega}_d \backslash \bar{\Gamma}_d$, but may be discontinuous across $\bar{\Gamma}_d$. For SVEs in $\bar{\Omega}_r$, we use the ansatz from conventional first order homogenization given by Equation (4.4). However, for SVEs located on $\bar{\Gamma}_d$, we adopt a smeared approach, whereby the strain contribution from the displacement jump is smeared over l_d. Hence, we define

$$\boldsymbol{u}^{\mathrm{M}} = \bar{\boldsymbol{\epsilon}}_d|_{\bar{\boldsymbol{x}}} \cdot [\boldsymbol{x} - \bar{\boldsymbol{x}}] \text{ inside } \Omega_\square(\bar{\boldsymbol{x}}),\ \forall \bar{\boldsymbol{x}} \in \bar{\Gamma}_d, \tag{4.8}$$

where

$$\bar{\boldsymbol{\epsilon}}_d \stackrel{\text{def}}{=} \bar{\boldsymbol{\epsilon}}_0 + \frac{1}{2l_d} \left([\![\bar{\boldsymbol{u}}]\!] \otimes \boldsymbol{n} + \boldsymbol{n} \otimes [\![\bar{\boldsymbol{u}}]\!] \right), \tag{4.9}$$

and $\bar{\boldsymbol{\epsilon}}_0$ denotes the bulk strain on $\bar{\Gamma}_d$[1].

Using the integral transformations in Equations (4.3) and (4.7), together with the prolongation expressions in Equations (4.4) and (4.8), we may now restate Equation (4.1) as the macroscale problem of finding $\bar{\boldsymbol{u}} \in \bar{\mathbb{U}}$ such that

$$\int_{\bar{\Omega}_r} \bar{\boldsymbol{\sigma}}\{\bar{\boldsymbol{\epsilon}}\} : \delta\bar{\boldsymbol{\epsilon}} \, \mathrm{d}\Omega + \int_{\bar{\Gamma}_d} l_d \bar{\boldsymbol{\sigma}}\{\bar{\boldsymbol{\epsilon}}_d\} : \delta\bar{\boldsymbol{\epsilon}}_d \, \mathrm{d}\Gamma = \int_{\Gamma_{ext,N}} \hat{\boldsymbol{t}} \cdot \delta\bar{\boldsymbol{u}} \, \mathrm{d}\Gamma \quad \forall \delta\bar{\boldsymbol{u}} \in \bar{\mathbb{U}}^0, \tag{4.10}$$

where the effective macroscale stress $\bar{\boldsymbol{\sigma}}$ is (still) obtained from the microscale solution according to Equation (4.6).

Considering Equation (4.10) and recalling the definition of $\bar{\Omega}_r$ in Figure 4.3, we note that the macroscale finite element mesh will typically be a discretization of $\hat{\Omega}$ rather than $\bar{\Omega}_r$. Hence, the integral over $\bar{\Omega}_r$ in Equation (4.10) is inconvenient to evaluate from a computational perspective. To overcome this issue, recall the definition $\hat{\Omega} \stackrel{\text{def}}{=} \bar{\Omega}_r \cup \bar{\Omega}_d \setminus \bar{\Gamma}_d$ and let $\hat{\Omega}_d \stackrel{\text{def}}{=} \bar{\Omega}_d \setminus \bar{\Gamma}_d$. Elaborating the left hand side of Equation (4.10) using the expression $\int_{\bar{\Omega}_r} \bullet \, \mathrm{d}\Omega = \int_{\hat{\Omega}} \bullet \, \mathrm{d}\Omega - \int_{\bar{\Gamma}_d} l_d \bullet \, \mathrm{d}\Gamma$ yields (cf. Paper E)

$$\begin{aligned} \int_{\bar{\Omega}_r} \bar{\boldsymbol{\sigma}}\{\bar{\boldsymbol{\epsilon}}\} : \delta\bar{\boldsymbol{\epsilon}} \, \mathrm{d}\Omega + \int_{\bar{\Gamma}_d} l_d \bar{\boldsymbol{\sigma}}\{\bar{\boldsymbol{\epsilon}}_d\} : \delta\bar{\boldsymbol{\epsilon}}_d \, \mathrm{d}\Gamma = \\ \int_{\hat{\Omega}} \bar{\boldsymbol{\sigma}}\{\bar{\boldsymbol{\epsilon}}\} : \delta\bar{\boldsymbol{\epsilon}} \, \mathrm{d}\Omega + \int_{\bar{\Gamma}_d} l_d \left(\bar{\boldsymbol{\sigma}}\{\bar{\boldsymbol{\epsilon}}_d\} - \bar{\boldsymbol{\sigma}}\{\bar{\boldsymbol{\epsilon}}_0\} \right) : \delta\bar{\boldsymbol{\epsilon}} \, \mathrm{d}\Gamma + \int_{\bar{\Gamma}_d} \bar{\boldsymbol{\sigma}}\{\bar{\boldsymbol{\epsilon}}_d\} : \left([\![\delta\bar{\boldsymbol{u}}]\!] \otimes \boldsymbol{n} \right)^{sym} \mathrm{d}\Gamma, \end{aligned} \tag{4.11}$$

[1]The bulk strain on $\bar{\Gamma}_d$ is defined as the average of the limit values on each side of the interface.

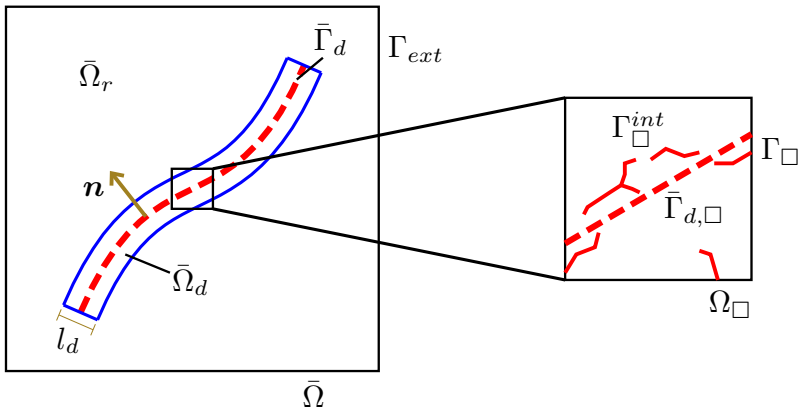

Figure 4.3: *Macroscopic domain $\bar{\Omega}$ divided into a part $\bar{\Omega}_d$ containing an effective macroscopic discontinuity $\bar{\Gamma}_d$, and a part $\bar{\Omega}_r$ that is free from macroscopic discontinuities.*

where we also used that $\delta\bar{\boldsymbol{\epsilon}}_d = \delta\bar{\boldsymbol{\epsilon}}_0 + \frac{1}{l_d}\left(\llbracket\delta\bar{\boldsymbol{u}}\rrbracket \otimes \boldsymbol{n}\right)^{sym}$. Inserting the result from Equation (4.11) in Equation (4.10), the macroscale problem is then to find $\bar{\boldsymbol{u}} \in \bar{\mathbb{U}}$ such that

$$\bar{a}\left(\bar{\boldsymbol{u}}, \delta\bar{\boldsymbol{u}}\right) = l\left(\delta\bar{\boldsymbol{u}}\right) \;\; \forall \delta\bar{\boldsymbol{u}} \in \bar{\mathbb{U}}^0, \tag{4.12}$$

where

$$\bar{a}\left(\bar{\boldsymbol{u}}, \delta\bar{\boldsymbol{u}}\right) = \underbrace{\int_{\hat{\Omega}} \bar{\boldsymbol{\sigma}}\{\bar{\boldsymbol{\epsilon}}\} : \delta\bar{\boldsymbol{\epsilon}} \, \mathrm{d}\Omega}_{\stackrel{\text{def}}{=} I_1} + \underbrace{\int_{\bar{\Gamma}_d} l_d \left(\bar{\boldsymbol{\sigma}}\{\bar{\boldsymbol{\epsilon}}_d\} - \bar{\boldsymbol{\sigma}}\{\bar{\boldsymbol{\epsilon}}_0\}\right) : \delta\bar{\boldsymbol{\epsilon}} \, \mathrm{d}\Gamma}_{\stackrel{\text{def}}{=} I_2} + \underbrace{\int_{\bar{\Gamma}_d} \bar{\boldsymbol{\sigma}}\{\bar{\boldsymbol{\epsilon}}_d\} : \left(\llbracket\delta\bar{\boldsymbol{u}}\rrbracket \otimes \boldsymbol{n}\right)^{sym} \mathrm{d}\Gamma}_{\stackrel{\text{def}}{=} I_3}. \tag{4.13}$$

We note that the term I_2 is scaled by l_d, and therefore will be negligible for sufficiently small l_d. See Paper E for further details.

4.4 Macroscale crack initiation

When softening of the effective SVE response occurs due to damage evolution, a macroscopic crack needs to be initiated. To facilitate macroscale crack initiation, we need to *i)* detect the onset of macroscopic softening and *ii)* determine the orientation of the macroscopic discontinuity surface.

One way to detect macroscopic softening is to monitor the homogenized microscale tangent. In particular, two popular criteria exist for detection of strain localization:

singularity of the acoustic tensor and the strict ellipticity condition. These criteria can both be applied directly to the tangent stiffness, without further knowledge of the model that the tangent was computed from. Hence, the criteria can be applied in a multiscale setting as well as in single scale problems, as long as the bulk response exhibits softening. In the present work, we use the strict ellipticity condition to detect macroscopic softening and to identify the discontinuity surface orientation. See Paper F for explicit mathematical expressions.

From a practical point of view, we remark that both localization criteria work well if the damage evolution is implicitly updated (i.e. if damage evolution is updated at the new time step), whereas additional modeling would be needed for explicitly updated damage evolution (i.e. if the damage is taken from the old time step and updated in a staggered fashion). A typical example of the latter situation is when microscale damage is represented entirely by propagation of traction free XFEM cracks, whereby a popular approach is to propagate the XFEM cracks at the end of each time step. In this case, the tangent stiffness will remain elliptic during any time step and loss of ellipticity based on the tangent stiffness can therefore not be used to detect strain localization.

Finally, we remark that the initiation of a macroscopic discontinuity only facilitates the development of a possible crack. The framework presented in Section 4.3 is valid even if no fracture develops along $\bar{\Gamma}_d$.

5 Localization aligned weakly periodic boundary conditions

5.1 Preliminaries

To solve the microscale problem obtained from Equation (4.2) on an SVE $\Omega_\square$, the macroscopic part of the displacement given by Equation (4.4) or Equation (4.8) is imposed on the SVE boundary through suitable boundary conditions (BCs). To this end, it would (in principle) be possible to use Dirichlet BCs or strong periodic BCs, but an extremely large SVE would be required due to the artificial crack closure on the boundaries arising with these BCs (cf. Paper B). Using Neumann BCs would, however, not give reliable results, because such BCs may lead to spurious softening (see Paper B or [9]). To obtain accurate results with smaller SVEs than required by Dirichlet or strong periodic BCs, we have developed weakly periodic boundary conditions that are aligned to the dominating localization direction in the SVE (Paper A, B and D).

5.2 Microscale problem

To impose the effective strain $\bar{\boldsymbol{\epsilon}}$ on the SVE by means of weakly periodic boundary conditions, we divide the SVE boundary into an image part $\Gamma_\square^+$ and a mirror part $\Gamma_\square^-$ as shown in Figure 5.1. Furthermore, we introduce a mapping[1] $\boldsymbol{\varphi}_{per} : \Gamma_\square^+ \to \Gamma_\square^-$ such that

[1]The actual construction of $\boldsymbol{\varphi}_{per}$ is discussed later.

points on $\Gamma_{\square}^{+}$ and $\Gamma_{\square}^{-}$ are associated to each other according to $\boldsymbol{x}^{-} = \boldsymbol{\varphi}_{per}(\boldsymbol{x}^{+})$ as also shown in Figure 5.1. We define the jump between a point $\boldsymbol{x}^{+}$ on $\Gamma_{\square}^{+}$ and the associated point $\boldsymbol{x}^{-} = \boldsymbol{\varphi}_{per}(\boldsymbol{x}^{+})$ on $\Gamma_{\square}^{-}$ as

$$[\![\boldsymbol{u}]\!]_{\square} \overset{\text{def}}{=} \boldsymbol{u}\left(\boldsymbol{x}^{+}\right) - \boldsymbol{u}\left(\boldsymbol{x}^{-}\right) = \boldsymbol{u}\left(\boldsymbol{x}^{+}\right) - \boldsymbol{u}\left(\boldsymbol{\varphi}_{per}\left(\boldsymbol{x}^{+}\right)\right).$$

Next, we impose weakly periodic boundary conditions on the SVE by introducing an independent discretization for the boundary traction $\boldsymbol{t}_{\lambda}$ and requiring $[\![\boldsymbol{u}]\!]_{\square} = \bar{\boldsymbol{\epsilon}} \cdot [\![\boldsymbol{x} - \bar{\boldsymbol{x}}]\!]_{\square}$ to hold in a weak sense. The SVE problem is then to find $\boldsymbol{u} \in \mathbb{U}_{\square}$ and $\boldsymbol{t}_{\lambda} \in \mathbb{T}_{\square}$ such that

$$\begin{aligned} a_{\square}(\boldsymbol{u}, \delta\boldsymbol{u}) - d_{\square}(\boldsymbol{t}_{\lambda}, \delta\boldsymbol{u}) &= 0 \;\; \forall \delta\boldsymbol{u} \in \mathbb{U}_{\square}, \\ -d_{\square}(\delta\boldsymbol{t}_{\lambda}, \boldsymbol{u}) &= -d_{\square}(\delta\boldsymbol{t}_{\lambda}, \bar{\boldsymbol{\epsilon}} \cdot [\boldsymbol{x} - \bar{\boldsymbol{x}}]) \;\; \forall \delta\boldsymbol{t}_{\lambda} \in \mathbb{T}_{\square}, \end{aligned} \tag{5.1}$$

$$\mathbb{U}_{\square} = \{\boldsymbol{v} : \boldsymbol{v} \in \left[\mathbb{H}^{1}(\Omega_{\square})\right]^{d}, \; \int_{\Gamma_{\square}} \boldsymbol{v} \, \mathrm{d}\Gamma = \boldsymbol{0}\}, \tag{5.2}$$

$$\mathbb{T}_{\square} = \{\boldsymbol{t} : \boldsymbol{t} \in \left[\mathbb{L}_{2}\left(\Gamma_{\square}^{+}\right)\right]^{(d)}\}, \tag{5.3}$$

where we introduced the expressions

$$a_{\square}(\boldsymbol{u}, \delta\boldsymbol{u}) \overset{\text{def}}{=} \frac{1}{|\Omega_{\square}|}\left[\int_{\Omega_{\square}} \boldsymbol{\sigma} : \boldsymbol{\epsilon}[\delta\boldsymbol{u}] \, \mathrm{d}\Omega - \int_{\Gamma_{\square,int}^{+}} \boldsymbol{t} \cdot [\![\delta\boldsymbol{u}]\!] \, \mathrm{d}\Gamma\right], \tag{5.4}$$

$$d_{\square}(\boldsymbol{t}_{\lambda}, \delta\boldsymbol{u}) \overset{\text{def}}{=} \frac{1}{|\Omega_{\square}|}\int_{\Gamma_{\square}^{+}} \boldsymbol{t}_{\lambda} \cdot [\![\delta\boldsymbol{u}]\!]_{\square} \, \mathrm{d}\Gamma. \tag{5.5}$$

Here, $\mathbb{L}_{2}\left(\Gamma_{\square}^{+}\right)$ denotes the space of square integrable functions on $\Gamma_{\square}^{+}$, $\mathbb{H}^{1}(\Omega_{\square})$ denotes the space of square integrable functions with square integrable derivatives in $\Omega_{\square}$, and d is the number of spatial dimensions.

Solving Equation (5.1) and employing Equation (4.6) allows $\bar{\boldsymbol{\sigma}} = \bar{\boldsymbol{\sigma}}\{\bar{\boldsymbol{\epsilon}}\}$ to be computed. We remark that, in $\bar{\Omega}_{d}$, the weakly periodic boundary conditions are employed to impose the macroscopic strain $\bar{\boldsymbol{\epsilon}}_{d} = \bar{\boldsymbol{\epsilon}}_{0} + \frac{1}{l_{d}}\left([\![\bar{\boldsymbol{u}}]\!] \otimes \boldsymbol{n}\right)^{sym}$ in a weak sense on the whole SVE boundary. Hence, there is no need to explicitly identify the location or width of the damaged zone in the SVE, only the localization direction needs to be determined in order to define the normal $\boldsymbol{n}$ of the effective discontinuity.

So far, we have not discussed the actual expression for the mirror function $\boldsymbol{\varphi}_{per}$. The standard choice for $\boldsymbol{\varphi}_{per}$, which is used in Paper A and Paper B as well as by [53] among many others, is to map points along horizontal or vertical lines as shown in Figure 5.1a. However, as pointed out by several researchers [5, 9, 55], this choice leads to inaccurate results in some situations. In particular, it works well if cracks or localization bands are aligned with the periodicity directions, whereas artificial crack closure occurs on the SVE boundary for cracks that are not aligned with these directions. The standard mirror function is shown in Figure 5.1a and corresponds to stacking SVEs as shown in Figure 5.2b. For the 2D case, the standard mirror function can be explicitly expressed as

$$\begin{aligned} \boldsymbol{\varphi}_{per}(l_{\square}, y) &= (0, y), \\ \boldsymbol{\varphi}_{per}(x, l_{\square}) &= (x, 0), \end{aligned} \tag{5.6}$$

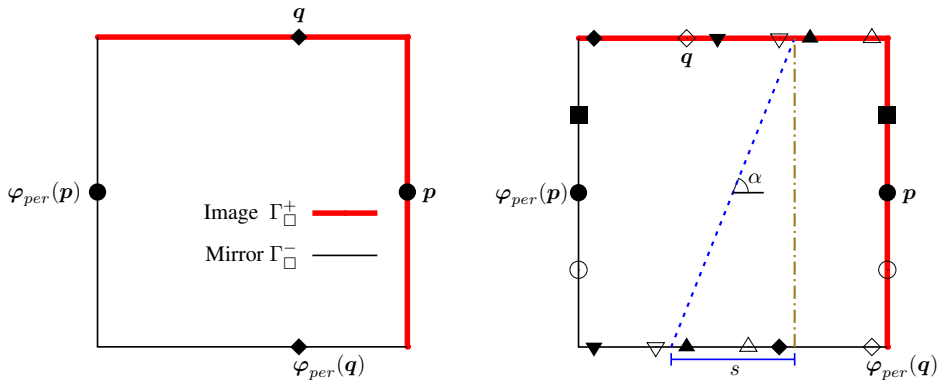

(a) *Standard mirror function.*

(b) *Shifted mirror function. The shifting distance* s *is given by* $s = l_\square / \tan\alpha$.

Figure 5.1: *SVE with boundary divided into an image part* $\Gamma^+_\square$ *and a mirror part* $\Gamma^-_\square$*, with standard mirror function (a) and shifted mirror function (b), where the shifting distance is given by* $s = l_\square / \tan\alpha$*. The symbols denote related points on* $\Gamma^+_\square$ *and* $\Gamma^-_\square$.

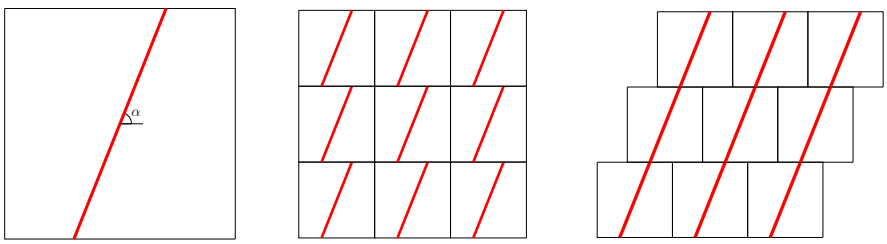

(a) *SVE with crack.*

(b) *Standard stacking.*

(c) *Shifted stacking.*

Figure 5.2: *An SVE with a crack (a), subjected to standard stacking (b) and shifted stacking (c).*

where $l_\square$ denotes the side length of the SVE.

An alternative to the standard mirror function given by Equation (5.6) can be developed by assuming that a dominating crack or localization band direction exists as indicated in Figure 5.1b and Figure 5.2a. By considering a shifted stacking as shown in Figure 5.2c, the crack pattern is compatible over SVE boundaries, and this compatibility prevents artificial crack closure. To obtain the shifted stacking shown in Figure 5.2c, the mirror function is modified as shown in Figure 5.1b, where some points on $\Gamma^+_\square$ are no longer mapped along vertical or horizontal lines. For the 2D case, the explicit expression for

$\boldsymbol{\varphi}_{per}$ as shown in Figure 5.1b is given by

$$\begin{aligned}
&\boldsymbol{\varphi}_{per}\left(l_{\square}, y\right) = (0, y), \\
&\boldsymbol{\varphi}_{per}\left(x, l_{\square}\right) = (l_{\square} - s + x, 0) \text{ if } 0 \leq x < s, \\
&\boldsymbol{\varphi}_{per}\left(x, l_{\square}\right) = (x - s, 0) \text{ if } s \leq x \leq l_{\square},
\end{aligned} \tag{5.7}$$

where the shifting distance is given by $s = l_{\square}/\tan\alpha$. Clearly, we may carry out the same procedure also for cracks with $\alpha < 45°$, whereby the SVEs would be shifted in the vertical direction rather than in the horizontal direction.

Using the expression given by Equation (5.7), we may obtain aligned periodic boundary conditions on weak form by only modifying the mirror function $\boldsymbol{\varphi}_{per}$. Note that the shifting distance s depends only on α and $l_{\square}$. Hence, the shifting is valid also for cracks that do not pass through the center of the SVE. See Paper D for further details.

Remark: The shifted stacking proposed here can be applied also in 3D, whereby shifting in two directions is necessary as compared to the 2D case, where shifting in one direction is sufficient. See Figure 5.3 for a schematic illustration.

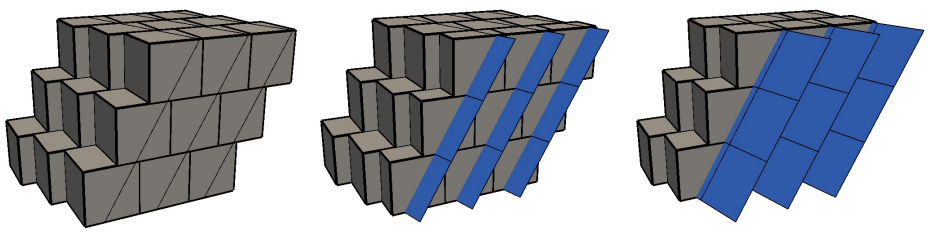

Figure 5.3: *Shifted stacking in 3D. SVEs colored in gray and cracks colored in blue.*

5.3 Traction discretization

Equation (5.1) defines the microscale problem with weakly periodic BCs. A main advantage of weakly periodic BCs compared to standard periodic BCs, in addition to not requiring a periodic mesh, is the possibility to choose the traction discretization $\mathbb{T}^h_{\square} \subset \mathbb{T}_{\square}$. In particular, the traction discretization can be adapted to the problem at hand in order to gain improved convergence with increasing SVE size.

To exploit the advantages of weakly periodic BCs, the construction of $\mathbb{T}^h_{\square}$ deserves further attention. Possible options for $\mathbb{T}^h_{\square}$ is to use a global polynomial basis [56] or a traction mesh on the SVE boundary [53]. To facilitate adaption of the traction mesh to the topology of cracks in the SVE, we choose the latter option. We now restrict the discussion to problems in 2D. Hence, we construct a (one-dimensional) traction mesh on $\Gamma^+_{\square}$, defined by traction nodes and two-node traction elements. The traction is then assumed to be piecewise constant or piecewise linear on each traction element.

To construct the traction mesh, we start from the approach in [53], where the first step is to project all (displacement) nodes on the image boundary as well as the mirror boundary onto the image boundary, as shown in Figure 5.4. Points where cracks or other possible discontinuities (such as e.g. grain boundaries of a poly crystal) intersect the boundary are projected in the same way. Next, points that are closer to each other than a given tolerance are merged, in order to prevent that traction elements become too small. If voids intersect the boundary, traction elements over the voids are removed. Performing these steps results in a dense traction mesh that can be used as it is, or coarsened as indicated to the right in Figure 5.4.

A particular choice for the traction mesh, that has shown promising results in the present work, is a coarse piecewise constant traction approximation. More precisely, the traction mesh is coarsened so much that only traction nodes at SVE corners and crack-boundary intersections are retained as shown in Figure 5.5. This approximation often performs very well, as shown in Paper A and Paper B, and the approximation can be combined with the modified mirror function discussed in Paper D. Since a mixed formulation is employed, the inf-sup (LBB) condition needs to be fulfilled. In Paper A, we show analytically that this particular choice of piecewise constant traction approximation indeed fulfills the inf-sup condition.

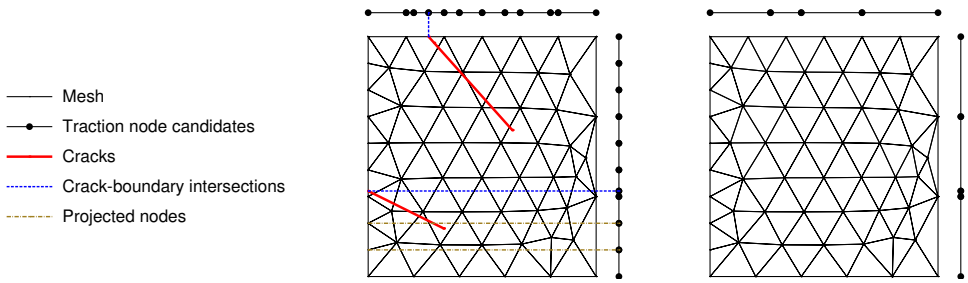

Figure 5.4: *Traction discretization: unprocessed (left) and processed (right) traction meshes. Addition of traction nodes where cracks intersect the boundary is indicated to the left.*

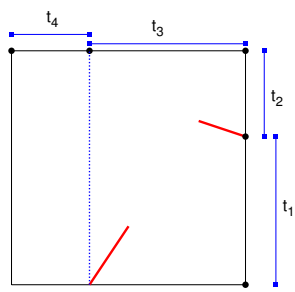

Figure 5.5: *Piecewise constant traction approximation with traction discontinuities at SVE boundaries and crack-boundary intersections.*

5.4 Effective stiffness

To solve the macroscale problem given by Equation (4.12), where $\bar{\boldsymbol{\sigma}}\{\bar{\boldsymbol{\epsilon}}\}$ is obtained on-the-fly from SVE solutions, we also need to compute the effective stiffness $\bar{\mathbf{C}} = \frac{\partial \bar{\boldsymbol{\sigma}}}{\partial \bar{\boldsymbol{\epsilon}}}$ from a given SVE solution. One option for computing $\bar{\mathbf{C}}$ is to perform condensation of the tangent from the SVE problem. To derive this condensation, note that in the last Newton iteration, where we have obtained convergence of the SVE problem, we solve

$$\begin{aligned} \underline{S}\Delta\underline{a}_u - \underline{C}\Delta\underline{a}_t &= 0, \\ -\underline{C}^T\Delta\underline{a}_u &= -\Delta\underline{f}, \end{aligned} \tag{5.8}$$

where $\Delta\underline{a}_u$ and $\Delta\underline{a}_t$ denote the increments in the SVE displacement and traction, respectively. Equation (5.8) is thus the discrete and linearized counterpart of Equation (5.1). More specifically, $\underline{S}$ is the "bulk stiffness" contribution pertaining to $a_\square(\boldsymbol{u}_h, \delta\boldsymbol{u}_h)$, $\underline{C}$ is the boundary traction contribution pertaining to $d_\square(\boldsymbol{t}_{\lambda,h}, \delta\boldsymbol{u}_h)$, and $\Delta\underline{f}$ is the linearization of the right hand side.

Now, consider the linearization of the effective stress $\bar{\boldsymbol{\sigma}}$ expressed (on Voigt format) in terms of the FE approximation according to

$$\Delta\left(\begin{bmatrix}\bar{\sigma}_{xx}\\ \bar{\sigma}_{yy}\\ \bar{\sigma}_{xy}\\ \bar{\sigma}_{yx}\end{bmatrix}\right) = \Delta\left(\frac{1}{|\Omega_\square|}\int_{\Gamma_\square}\begin{bmatrix}x & 0\\ 0 & y\\ 0 & x\\ y & 0\end{bmatrix}\begin{bmatrix}t_x\\ t_y\end{bmatrix}\mathrm{d}\Gamma\right) = \underbrace{\frac{1}{|\Omega_\square|}\int_{\Gamma_\square^+}\begin{bmatrix}[\![x]\!]_\square & 0\\ 0 & [\![y]\!]_\square\\ 0 & [\![x]\!]_\square\\ [\![y]\!]_\square & 0\end{bmatrix}\underline{N}_t\,\mathrm{d}\Gamma}_{\stackrel{\text{def}}{=}\underline{D}^T}\Delta\underline{a}_t, \tag{5.9}$$

where the matrix $\underline{N}_t$ contains the basis functions for the traction approximation. From Equation (5.8), we have

$$\Delta\underline{a}_t = \left(\underline{C}^T\underline{S}^{-1}\underline{C}\right)^{-1}\Delta\underline{f}, \tag{5.10}$$

which, combined with Equation (5.9), gives

$$\begin{bmatrix}\Delta\bar{\sigma}_{xx}\\ \Delta\bar{\sigma}_{yy}\\ \Delta\bar{\sigma}_{xy}\\ \Delta\bar{\sigma}_{yx}\end{bmatrix} = \underline{D}^T\left(\underline{C}^T\underline{S}^{-1}\underline{C}\right)^{-1}\Delta\underline{f}. \tag{5.11}$$

Taking the variation of the contribution from $\bar{\boldsymbol{\epsilon}}$ gives

$$\Delta\underline{f} = \underbrace{\frac{1}{|\Omega_\square|}\int_{\Gamma_\square^+}\underline{N}_t^T\begin{bmatrix}[\![x]\!]_\square & 0 & 0 & [\![y]\!]_\square\\ 0 & [\![y]\!]_\square & [\![x]\!]_\square & 0\end{bmatrix}\mathrm{d}\Gamma}_{=\underline{D}}\begin{bmatrix}\Delta\bar{\epsilon}_{xx}\\ \Delta\bar{\epsilon}_{yy}\\ \Delta\bar{\epsilon}_{xy}\\ \Delta\bar{\epsilon}_{yx}\end{bmatrix}. \tag{5.12}$$

Combining Equations (5.11) and (5.12) now gives the effective stiffness as

$$\begin{bmatrix} \Delta\bar{\sigma}_{xx} \\ \Delta\bar{\sigma}_{yy} \\ \Delta\bar{\sigma}_{xy} \\ \Delta\bar{\sigma}_{yx} \end{bmatrix} = \underbrace{\left(\underline{D}^T \left(\underline{C}^T \underline{S}^{-1} \underline{C}\right)^{-1} \underline{D}\right)}_{\bar{\mathbf{C}}} \begin{bmatrix} \Delta\bar{\epsilon}_{xx} \\ \Delta\bar{\epsilon}_{yy} \\ \Delta\bar{\epsilon}_{xy} \\ \Delta\bar{\epsilon}_{yx} \end{bmatrix}. \tag{5.13}$$

6 Numerical implementation

In the present work, the following open source software packages have been used extensively:

- The models developed in the present work have been implemented in OOFEM [57, 58] and can be downloaded from `https://github.com/erisve/oofem`. OOFEM is object oriented and written in C++. It comes with an automatic test suite (roughly 250 tests) and version control using Git. Apart from the present work, OOFEM has also been used for computational homogenization in [56, 59, 60, 61, 62, 63].
- The grain structures considered in paper B were prepared using Neper [64, 65] and Phon [66]. Neper can be downloaded from `http://neper.sourceforge.net/` and Phon is available at `https://github.com/KristofferC/Phon`. Neper is written in C and Phon is written in Python.
- Salome [67] was used for mesh generation and can be downloaded from `http://www.salome-platform.org/`. It allows automated meshing using a Python interface.
- The post-processing was done with Paraview (`http://www.paraview.org/`) [68] and Gnuplot (http://www.gnuplot.info/) [69].

7 Summary of appended papers

7.1 Paper A: Computational homogenization of microfractured continua using weakly periodic boundary conditions

In Paper A, computational homogenization of an elastic material containing stationary microcracks is considered. The cracks are modeled using XFEM and weakly periodic BCs are developed for the SVE problem. The resulting weak formulation of the microscale problem has displacements and boundary tractions as unknowns, thereby allowing the boundary traction to be adapted to the geometry of the problem at hand. To exploit this possibility, we develop a traction approximation that is suitable when cracks intersect the SVE boundary. The main result of Paper A is the proposition of a stable traction approximation that is piecewise constant between crack-boundary intersections. We prove

analytically that the proposed approximation is stable in terms of the inf-sup (LBB) condition. The numerical examples show that the proposed traction approximation is more efficient than conventional boundary conditions (Dirichlet, Neumann, strong periodic) in terms of convergence with increasing SVE size.

7.2 Paper B: On computational homogenization of microscale crack propagation

The early stage of crack propagation, prior to macroscopic localization, is considered in Paper B. More precisely, the model developed in Paper A is extended to handle propagating cracks. For the modeling of crack propagation, we consider *i)* XFEM in combination with the concept of material forces to model elastic crack propagation and *ii)* conventional interface elements to model crystal grain debonding. The numerical examples show that weakly periodic boundary conditions, with piecewise constant traction approximation between crack-boundary intersections, are effective also when damage progression occurs in the microstructure.

7.3 Paper C: A weak penalty formulation remedying traction oscillations in interface elements

The spurious traction oscillations sometimes seen in interface elements are studied in Paper C. The study employs a weak penalty formulation, which shares stability properties with an equivalent mixed formulation. Based on this equivalence, oscillations in interface elements are explained by studying the inf-sup stability for the mixed formulation. Interestingly, it turns out that conventional interface elements (with full or reduced integration) correspond to approximations violating the inf-sup condition. In contrast, oscillation free results are obtained by choosing a stable approximation applied in the weak penalty setting, as shown by the numerical examples.

7.4 Paper D: Localization aligned weakly periodic boundary conditions

In Paper D, the boundary conditions developed in Paper A and Paper B are improved by aligning the periodicity directions with an effective localization direction. It turns out that this alignment can be achieved by only modifying the mapping (mirror function) between the associated parts of the SVE boundary. This modified mirror function leads to more accurate results than unaligned weakly periodic boundary conditions, as demonstrated by the numerical examples.

7.5 Paper E: Two-scale modeling of fracturing solids using a smeared macro-to-micro discontinuity transition

In Paper E, Variationally Consistent Homogenization (VCH) is employed to develop a two-scale scheme accounting for cracks on both scales. A continuous-discontinuous homogenization approach is adopted, whereby a macroscopic cohesive zone model is obtained from the response of the localized SVEs. A key feature of the proposed scheme is that the macroscopic displacement jump is applied in a smeared sense as an additional strain contribution on the localized SVE. The macroscale weak formulation contains a conventional cohesive zone contribution as well as a correction term containing the difference of the stresses in the localizing SVE and the unloading SVE. It turns out that this correction term, as well as the bulk strain contribution to the localizing SVE, can be neglected if the SVE is sufficiently small (i.e. if strong scale separation holds). The derived model is combined with the models developed in Papers A, B and D in order to obtain a scheme capable of handling macroscopic localization. The response predicted by the proposed scheme agrees well with DNS as demonstrated by the numerical examples.

7.6 Paper F: A two-scale model for strain localization in solids: XFEM procedures and computational aspects

In Paper E, we focused on cases where the position and orientation of macroscale localization bands could be determined a-priori. The model is therefore extended in Paper F to also consider the transition to strain localization on the macroscale. To this end, macroscale discontinuities are inserted based on the strict ellipticity condition. By combining this condition with the previously developed macro-to-micro transitions, we obtain a modeling framework capable of handling macroscopic localization. Since material models exhibiting softening are considered, Newton's method is generally not sufficiently robust. Therefore, we improve the robustness of the numerical simulations by employing trust-region methods on both scales. Furthermore, we discuss computational aspects of multiscale localization modeling using XFEM. A few numerical examples are given, demonstrating that the proposed scheme agrees well with the results obtained with predefined macrocracks.

8 Conclusions and outlook

The present work is concerned with multiscale modeling in the presence of cracks on the macroscale as well as on the microscale. In particular, we address the development of suitable boundary conditions (BCs) on the Statistical Volume Element (SVE) and the formulation of proper scale transitions for macroscopic cracks. Stability and robustness issues related to multiscale crack modeling are also discussed.

An interesting conclusion from the present work is that it is possible to outperform conventional BCs (including strong periodic BCs) in terms of convergence with increasing SVE size when cracks are present in the microstructure. This can be achieved within the setting of weakly periodic BCs by *i)* adapting the traction discretization to the problem at hand (Papers A, B), and *ii)* by aligning the periodicity with an identified localization direction (Paper D).

Regarding stability issues, a significant conclusion from the present work is that the traction oscillations sometimes seen in interface elements (for both full, two-point Lobatto and one-point integration) can be alleviated by using a weak penalty formulation (Paper C). More precisely, oscillation free results can be obtained by projecting the cohesive zone contribution onto a stable subspace. In the derivation of the weak penalty formulation, full integration, two-point Lobatto integration and reduced one point integration are identified as unstable special cases of the weak penalty formulation. This explains the oscillations occurring in some situations for these integration schemes.

By combining the models proposed in the present work, a two-scale scheme capable of handling macroscopic localization can be constructed (Papers E, F). The numerical examples show that the results obtained with the proposed scheme agree well with Direct Numerical Simulations (DNS). In contrast to previously published work, the scheme does not require dynamic tracking of an evolving damaged region in the SVE and does not require restrictive constitutive assumptions on the microscale.

Regarding future work, an interesting extension is to consider material models that better describe the microscale behavior of metals. A suitable candidate is crystal plasticity [70, 71] in combination with tailored crack propagation models [72] and models of the grain microstructure [65]. Furthermore, since the present work is restricted to 2D, a natural extension is to consider 3D models. For the extension to 3D, it can be noted that the alignment of weakly periodic BCs (Paper D) is easily extended to 3D, whereas the construction of an elaborate traction approximation (Papers A, B) is substantially more involved in the 3D case. We also note that the weak penalty formulation in Paper C can be trivially extended to 3D.

References

[1] T. Zohdi and P. Wriggers. A model for simulating the deterioration of structural-scale material responses of microheterogeneous solids. *Computer Methods in Applied Mechanics and Engineering* **190**.22-23 (2001), 2803–2823.

[2] J. Fish, K. Shek, M. Pandheeradi, and M. S. Shephard. Computational plasticity for composite structures based on mathematical homogenization: Theory and practice. *Computer Methods in Applied Mechanics and Engineering* **148**.1-2 (1997), 53–73.

[3] M. Ostoja-Starzewski. Material spatial randomness: From statistical to representative volume element. *Probabilistic Engineering Mechanics* **21**.2 (2006), 112–132.

[4] V. Kouznetsova, M. G. D. Geers, and W. A. M. Brekelmans. Multi-scale constitutive modelling of heterogeneous materials with a gradient-enhanced computational homogenization scheme. *International Journal for Numerical Methods in Engineering* **54**.8 (2002), 1235–1260.

[5] H. Talebi, M. Silani, S. P. A. Bordas, P. Kerfriden, and T. Rabczuk. A computational library for multiscale modeling of material failure. *Computational Mechanics* **53**.5 (2013), 1047–1071.

[6] M. G. D. Geers, V. G. Kouznetsova, and W. A. M. Brekelmans. Multi-scale computational homogenization: Trends and challenges. *Journal of Computational and Applied Mathematics* **234**.7 (2010), 2175–2182.

[7] V. P. Nguyen, M. Stroeven, and L. J. Sluys. Multiscale continuous and discontinuous modeling of heterogeneous materials: A review on recent developments. *Journal of Multiscale Modelling* **3**.04 (2011), 229–270.

[8] T. I. Zohdi and P. Wriggers. Introduction to computational micromechanics. *Lecture Notes in Applied and Computational Mechanics* **20** (2005).

[9] E. W. C. Coenen, V. G. Kouznetsova, and M. G. D. Geers. Novel boundary conditions for strain localization analyses in microstructural volume elements. *International Journal for Numerical Methods in Engineering* **90**.1 (2012), 1–21.

[10] M Jirásek. *Modeling of localized inelastic deformation (lecture notes)*. Tech. rep. Prague: Czech Technical University, 2010.

[11] R. de Borst. Computation of post-bifurcation and post-failure behavior of strain-softening solids. *Computers and Structures* **25**.2 (1987), 211–224.

[12] F. V. Souza and D. H. Allen. Modeling the transition of microcracks into macrocracks in heterogeneous viscoelastic media using a two-way coupled multiscale model. *International Journal of Solids and Structures* **48**.22-23 (2011), 3160–3175.

[13] V. P. Nguyen, O. Lloberas-Valls, M. Stroeven, and L. J. Sluys. Homogenization-based multiscale crack modelling: From micro-diffusive damage to macro-cracks. *Computer Methods in Applied Mechanics and Engineering* **200**.9-12 (2011), 1220–1236.

[14] C. V. Verhoosel, J. J. C. Remmers, M. A. Gutiérrez, and R. de Borst. Computational homogenization for adhesive and cohesive failure in quasi-brittle solids. *International Journal for Numerical Methods in Engineering* **83**.8-9 (2010), 1155–1179.

[15] T. Belytschko, S. Loehnert, and J. H. Song. Multiscale aggregating discontinuities: A method for circumventing loss of material stability. *International Journal for Numerical Methods in Engineering* **73**.6 (2008), 869–894.

[16] E. Bosco, V. G. Kouznetsova, and M. G. D. Geers. Multi-scale computational homogenization-localization for propagating discontinuities using X-FEM. *International Journal for Numerical Methods in Engineering* **102**.3-4 (2015), 496–527.

[17] E. W. C. Coenen, V. G. Kouznetsova, E. Bosco, and M. G. D. Geers. A multi-scale approach to bridge microscale damage and macroscale failure: a nested computational homogenization-localization framework. *International Journal of Fracture* **178**.1-2 (2012), 157–178.

[18] E. Bosco, V. G. Kouznetsova, E. W. C. Coenen, M. G. D. Geers, and A. Salvadori. A multiscale framework for localizing microstructures towards the onset of macroscopic discontinuity. *Computational Mechanics* **54**.2 (2014), 299–319.

[19] S. Toro, P. J. Sánchez, P. J. Blanco, E. A. De Souza Neto, A. E. Huespe, and R. A. Feijóo. Multiscale formulation for material failure accounting for cohesive cracks at the macro and micro scales. *International Journal of Plasticity* **76** (2016), 75–110.

[20] K. Runesson and F. Larsson. Adaptive Bridging of Scales in Continuum Modeling Based on Error Control. *International Journal for Multiscale Computational Engineering* **6**.4 (2008), 371–392.

[21] C. Miehe, F. Welschinger, and M. Hofacker. Thermodynamically consistent phase-field models of fracture: Variational principles and multi-field FE implementations. *International Journal for Numerical Methods in Engineering* **83**.10 (2010), 1273–1311.

[22] M. Ortiz and A. Pandolfi. Finite-deformation irreversible cohesive elements for three-dimensional crack-propagation analysis. *International Journal for Numerical Methods in Engineering* **44**.9 (1999), 1267–1282.

[23] T. Belytschko and T. Black. Elastic crack growth in finite elements with minimal remeshing. *International Journal for Numerical Methods in Engineering* **45**.5 (1999), 601–620.

[24] T. P. Fries and T Belytschko. The extended/generalized finite element method: an overview of the method and its applications. *International Journal for Numerical Methods in Engineering* **84**.3 (2010), 253–304.

[25] J. Lemaitre. *A course on damage mechanics*. Springer Berlin Heidelberg, 1996.

[26] P. Dumstorff and G. Meschke. Crack propagation criteria in the framework of X-FEM-based structural analyses. *International Journal for Numerical and Analytical Methods in Geomechanics* **31**.2 (2007), 239–259.

[27] G. Zi and T. Belytschko. New crack-tip elements for XFEM and applications to cohesive cracks. *International Journal for Numerical Methods in Engineering* **57**.15 (2003), 2221–2240.

[28] R. Larsson and M. Fagerström. A framework for fracture modelling based on the material forces concept with XFEM kinematics. *International Journal for Numerical Methods in Engineering* **62**.13 (2005), 1763–1788.

[29] M. Fagerström and R. Larsson. Approaches to dynamic fracture modelling at finite deformations. *Journal of the Mechanics and Physics of Solids* **56**.2 (2008), 613–639.

[30] V. P. Nguyen, O. Lloberas-Valls, M. Stroeven, and L. J. Sluys. Computational homogenization for multiscale crack modeling. Implementational and computational aspects. *International Journal for Numerical Methods in Engineering* **89**.2 (2012), 192–226.

[31] G. N. Wells. "Discontinuous modelling of strain localisation and failure". PhD thesis. Delft University of Technology, 2001.

[32] P. M. A. Areias and T. Belytschko. Analysis of three-dimensional crack initiation and propagation using the extended finite element method. *International Journal for Numerical Methods in Engineering* **63** (2005), 760–788.

[33] F. Larsson, K. Runesson, and F. Su. Variationally consistent computational homogenization of transient heat flow. *International Journal for Numerical Methods in Engineering* **81**.13 (2010), 1659–1686.

[34] D. Ngo and A. C. Scordelis. Finite Element Analysis of Reinforced Concrete Beams. *Journal of the American Concrete Institute* **64**.3 (1967), 152–163.

[35] R. de Borst, M. A. Crisfield, J. J. C. Remmers, and C. V. Verhoosel. *Non-Linear Finite Element Analysis of Solids and Structures: Second Edition*. John Wiley and Sons, 2012.

[36] X. P. Xu and A. Needleman. Numerical simulations of fast crack growth in brittle solids. *Journal of the Mechanics and Physics of Solids* **42**.9 (1994), 1397–1434.

[37] G. T. Camacho and M. Ortiz. Computational modelling of impact damage in brittle materials. *International Journal of Solids and Structures* **33**.20-22 (1996), 2899–2938.

[38] M. Samimi, J. A. W. van Dommelen, and M. G. D. Geers. A three-dimensional self-adaptive cohesive zone model for interfacial delamination. *Computer Methods in Applied Mechanics and Engineering* **200**.49-52 (2011), 3540–3553.

[39] T. Belytschko, N. Moës, S. Usui, and C. Parimi. Arbitrary discontinuities in finite elements. *International Journal for Numerical Methods in Engineering* **50**.4 (2001), 993–1013.

[40] N. Moës, J. Dolbow, and T. Belytschko. A finite element method for crack growth without remeshing. *International Journal for Numerical Methods in Engineering* **46**.1 (1999), 131–150.

[41] C. Daux, N. Moës, J. Dolbow, N. Sukumar, and T. Belytschko. Arbitrary branched and intersecting cracks with the extended finite element method. *International Journal for Numerical Methods in Engineering* **48**.12 (2000), 1741–1760.

[42] T. P. Fries and M. Baydoun. Crack propagation with the extended finite element method and a hybrid explicit-implicit crack description. *International Journal for Numerical Methods in Engineering* **89**.12 (2012), 1527–1558.

[43] J. C. J. Schellekens and R. De Borst. On the numerical integrations of interface elements. *International Journal for Numerical Methods in Engineering* **36**.1 (1993), 43–66.

[44] V. Kaliakin and J. Li. Insight into deficiencies associated with commonly used zero-thickness interface elements. *Computers and Geotechnics* **17**.2 (1995), 225–252.

[45] A. Simone. Partition of unity-based discontinuous elements for interface phenomena: computational issues. *Communications in Numerical Methods in Engineering* **20**.6 (2004), 465–478.

[46] A. Khoei, H. Azadi, and H. Moslemi. Modeling of crack propagation via an automatic adaptive mesh refinement based on modified superconvergent patch recovery technique. *Engineering Fracture Mechanics* **75**.10 (2008), 2921–2945.

[47] J. Dolbow, N. Moës, and T. Belytschko. Discontinuous enrichment in finite elements with a partition of unity method. *Finite Elements in Analysis and Design* **36**.3-4 (2000), 235–260.

[48] P. Steinmann, D. Ackermann, and F. Barth. Application of material forces to hyperelastostatic fracture mechanics. II. Computational setting. *International Journal of Solids and Structures* **38**.32-33 (2001), 5509–5526.

[49] J. Brouzoulis, F. Larsson, and K. Runesson. Strategies for planar crack propagation based on the concept of material forces. *Computational Mechanics* **47**.3 (2010), 295–304.

[50] T. Hettich, A. Hund, and E. Ramm. Modeling of failure in composites by X-FEM and level sets within a multiscale framework. *Computer Methods in Applied Mechanics and Engineering* **197**.5 (2008), 414–424.

[51] A. Ibrahimbegovic. *Nonlinear solid mechanics*. Vol. 160. Solid Mechanics and its Applications. Dordrecht: Springer Netherlands, 2009, pp. 1–594.

[52] K. Runesson and F. Larsson. Adaptive Bridging of Scales in Continuum Modeling Based on Error Control. *International Journal for Multiscale Computational Engineering* **6**.4 (2008), 371–392.

[53] F. Larsson, K. Runesson, S. Saroukhani, and R. Vafadari. Computational homogenization based on a weak format of micro-periodicity for RVE-problems. *Computer Methods in Applied Mechanics and Engineering* **200**.1-4 (2011), 11–26.

[54] T. J. R. Hughes, G. R. Feijóo, L. Mazzei, and J. B. Quincy. The variational multiscale method - A paradigm for computational mechanics. *Computer Methods in Applied Mechanics and Engineering* **166**.1-2 (1998), 3–24.

[55] S. D. Mesarovic and J. Padbidri. Minimal kinematic boundary conditions for simulations of disordered microstructures. *Philosophical Magazine* **85**.1 (2005), 65–78.

[56] C. Sandström, F. Larsson, and K. Runesson. Weakly Periodic Boundary Conditions for the Homogenization of Flow in Porous Media. *Advanced Modeling and Simulation in Engineering Sciences* **1**.1 (2014), 12.

[57] B Patzák and Z Bittnar. Design of object oriented finite element code. *Advances in Engineering Software* **32**.10-11 (2001), 759–767.

[58] B. Patzák. *OOFEM project home page: www.oofem.org*. 2000.

[59] C. Sandström, F. Larsson, K. Runesson, and H. Johansson. A two-scale finite element formulation of Stokes flow in porous media. *Computer Methods in Applied Mechanics and Engineering* **261-262** (2013), 96–104.

[60] C. Sandström, F. Larsson, and K. Runesson. Homogenization of coupled flow and deformation in a porous material. *Computer Methods in Applied Mechanics and Engineering* **308** (2016), 535–551.

[61] C. Sandström and F. Larsson. On bounded approximations of periodicity for computational homogenization of Stokes flow in porous media. *International Journal for Numerical Methods in Engineering* **109**.3 (2016).

[62] M. Öhman, K. Runesson, and F. Larsson. On the variationally consistent computational homogenization of elasticity in the incompressible limit. *Advanced Modeling and Simulation in Engineering Sciences* **2**.1 (2015), 1–29.

[63] M. Öhman, F. Larsson, and K. Runesson. Computational homogenization of liquid-phase sintering with seamless transition from macroscopic compressibility to incompressibility. *Computer Methods in Applied Mechanics and Engineering* **266** (2013), 219–228.

[64] R. Quey. *Neper project home page: http://neper.sourceforge.net*.

[65] R. Quey, P. Dawson, and F. Barbe. Large-scale 3D random polycrystals for the finite element method: Generation, meshing and remeshing. *Computer Methods in Applied Mechanics and Engineering* **200**.17-20 (2011), 1729–1745.

[66] K. Carlsson. *Phon project home page: https://github.com/KristofferC/Phon.git*.

[67] Salome. *Salome web page: www.salome-platform.org*.

[68] Paraview. *Paraview web page: www.paraview.org*.

[69] Gnuplot. *Gnuplot web page: www.gnuplot.info*.

[70] M. Ekh, R. Lillbacka, and K. Runesson. A model framework for anisotropic damage coupled to crystal (visco)plasticity. *International Journal of Plasticity* **20**.12 (2004), 2143–2159.

[71] S. Bargmann, B. Svendsen, and M. Ekh. An extended crystal plasticity model for latent hardening in polycrystals. *Computational Mechanics* **48**.6 (2011), 631–645.

[72] R. Lillbacka, E. Johnson, and M. Ekh. A model for short crack propagation in polycrystalline materials. *Engineering Fracture Mechanics* **73**.2 (2006), 223–232.